

# Finite-Element Modeling and Analysis of Reinforced Concrete Box Culverts

Anil K. Garg<sup>1</sup> and Ali Abolmaali<sup>2</sup>

**Abstract:** There have been several controversies with regard to the true behavior of reinforced concrete box culverts in recent years. To be able to conduct a parametric study to develop design equations, a complete three-dimensional verified finite-element model of culverts is essential. This study presents the development of an analytical program to investigate the shear capacity of precast reinforced concrete box culverts. To simulate the experimental results, complete and detailed three-dimensional finite-element models (FEMs) of the test specimens were developed and analyzed. Three-dimensional shell and solid elements were used to model the culvert systems. The welded wire fabrics were modeled by using the rebar elements placed on the surface elements provided by the ABAQUS software. The contact surface between the outside face of the bottom slab and reaction floor was modeled by using a nonlinear node-to-surface contact analysis procedure. The analysis procedure consisted of an incremental loading history to capture the problem of nonlinearity. The load was placed at a distance  $d$  from the tip of the haunch of the box culvert, where  $d$  is the effective depth of tension reinforcement at mid span, in the top slab of the box culvert. To simulate the wheel load a 25.4 cm (10 in.) $\times$ 51 cm (20 in.) plate is used experimentally as well as in finite-element modeling, which is used by AASHTO to model the wheel load of a HS20 truck. The smeared crack model along with the Riks analysis procedure were incorporated to analyze the system for microcracks and to stabilize the solution, respectively. The converged solution was obtained by using  $H$  convergence coupled with the difference between the external work done and the strain energy density of the system. The load-deflection plots obtained from the FEM analyses were compared with those obtained from the experimental results, which showed close correlation.

**DOI:** 10.1061/(ASCE)0733-947X(2009)135:3(121)

**CE Database subject headings:** Finite element method; Reinforced concrete; Culverts.

## Introduction

The precast concrete box culverts are manufactured in a range of standard span and rise, combinations. Box culvert sections are typically defined by their span, rise, and design height of fill as measured from finished grade to the top of the box section. The standard span per ASTM C 1433 2003 (ASTM 2003) varies from 0.91 to 3.66 m (3–12 ft) and the rise varies from 0.61 to 3.66 m (2–12 ft)—both in 0.3 m (1 ft) increments. The joint lengths vary as a function of the form equipment available to the producer, and they generally vary from 1.22 m (4 ft), as a practical minimum length, up to 2.44 m (8 ft). The inside corners of the walls and slabs are tapered to create a haunch, which has equal dimensions horizontally and vertically. The haunch dimension is equal to the wall thickness though some producers utilize form equipment, which yields a fixed haunch dimension [usually either 203 mm (8 in.) or 305 mm (12 in.)].

To study the behavior of all the possible standard box culverts,

three-dimensional (3D) finite-element models (FEMs) were prepared for all the standard sizes of box culverts per ASTM C 1433-04. The models included 3D solid and 3D shell elements having geometric and material nonlinearities. The reinforcement was modeled as rebar elements embedded in the surface element. The base support (strong reaction floor) was also modeled by modeling a rectangular block with a high value of stiffness. This was done to model the full-scale experimental test results conducted by Garg et al. (2006), Garg (2007), Garg and Abolmaali (2006), and Abolmaali and Garg (2006, 2008a,b). The contact regions between the box and the reaction floor were modeled by using node-to-surface contact elements. The boxes were loaded on an area equal to the wheel load plate 30 cm $\times$ 51 cm (10 in $\times$ 20 in). The incremental wheel load was applied by employing the Riks method (ABAQUS 2006) up to 445 kN (100 kip), the load at which most of the test specimens failed during experimental testing. The cracking strains were studied for all the load steps for all the 11-size boxes (Garg 2007) by using the FEM model built with brick (C3D8R) elements from the ABAQUS software. The amount of plastic strain needed to reduce the stresses to zero at the crack, which is known as tension stiffening, was used in controlling the stiffness of the model. The elements cracked at specified load levels were identified by using the cracking strain value.

## Load

The soil on the top of the top slab is neglected considering the worst case for the top slab of the box culvert as with soil, even

<sup>1</sup>Postdoctoral Fellow, Dept. of Civil and Environmental Engineering, Univ. of Texas at Arlington, Arlington TX 76019. E-mail: agarg.us@gmail.com

<sup>2</sup>Associate Professor, Dept. of Civil and Environmental Engineering, Univ. of Texas at Arlington, Arlington TX 76019 (corresponding author). E-mail: abolmaali@uta.edu

Note. Discussion open until August 1, 2009. Separate discussions must be submitted for individual papers. The manuscript for this paper was submitted for review and possible publication on June 15, 2008; approved on September 29, 2008. This paper is part of the *Journal of Transportation Engineering*, Vol. 135, No. 3, March 1, 2009. ©ASCE, ISSN 0733-947X/2009/3-121-128/\$25.00.

though the weight of soil might increase some of the load but will decrease the effect of wheel load substantially. The load of soil on the side walls has also been neglected as it also decreases the effect of the wheel load even though it is only by a small amount, which was checked separately. For the critical case the load was placed at a distance  $d$  from the tip of the haunch of the box culvert, where  $d$  is the effective depth of tension reinforcement at midspan, in the top slab of the box culvert. To simulate the wheel load a 25.4 cm (10 in.)  $\times$  51 cm (20 in.) plate is used experimentally as well as in finite-element modeling, which is used by AASHTO to model the wheel load of a HS20 truck.

## Elements

### Solid Element

Solid elements are volume elements, which are composed of a single homogeneous material, or can include several layers of different materials. Even though tetrahedral elements are relatively easy to model and cost effective when compared to hexahedral elements, hexahedral elements are shown to yield accurate results for linear and nonlinear analysis involving contact, plasticity, and large deformations. The first-order (linear) interpolation elements such as hexahedral (brick) exhibit potentially stiff behavior with a slow convergence rate but prevents potential “mesh locking” when a reduced integration analysis procedure is used, whereas second-order elements provide higher accuracy. However, first-order elements were used to accurately model the contact surfaces and prevent compact contact condition.

### Thick Shell Element

For all of the box except the haunch, the elements that were used are eight-noded quadrilateral in-plane general purpose continuum shell, reduced integration (SC8R), and finite membrane strains. These elements are capable of presenting results for the distribution of shear force and bending moments at various load levels in the models. They are also capable of accommodating rebar layers at the specified locations in the given part which are known as rebar elements. The stiffness of the rebar was transferred to the nearest nodes of the shell element. The bond slippage model was not considered, and perfect bond between the concrete and rebar was presumed. Thus, even after concrete cracking stiffness was available at the nodes due to the availability of steel at those nodes, their vicinity was reinforced until the failure rebar stress was reached. The shell element needed to be defined by using stacking and orientation direction. While meshing, each and every part of the model needed to be defined in the direction outside the box using the sweep mesh technique for correct model behavior. Since the haunch dimension is such that the width of the haunch varies (i.e., triangular shape), the “haunch” was modeled by using hexahedral brick elements.

### Brick Element

Thick shell elements were used to model the box culvert at all locations except for the haunch region. Thick shell elements were considered since they incorporate shear deformation in the element equations and they have the capacity (in ABAQUS) to directly show the bending moment and shear force contours. The latter is not the case for brick elements in ABAQUS. Since it was more difficult to model concrete cracking with a shell element, a

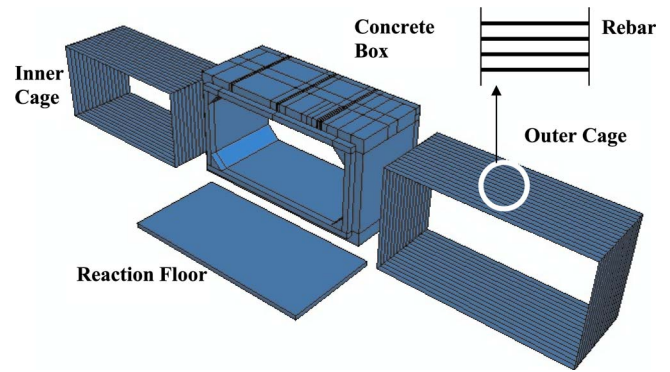


Fig. 1. FEM model parts showing inner cage, outer cage of rebar with concrete box, and strong reaction floor

separate model with reduced integration eight-noded linear brick elements (C3D8R) were used for predicting the cracking strain at various load levels in the model.

### Surface Element

Three-dimensional four-noded surface elements (SFM3D4) were used to accommodate the rebar elements. Stiffness and mass of the rebar layers were added to the surface elements. These reinforced surface elements were embedded in the brick (C3D8R) and thick shell (SC8R) “host” elements. Surface parts were generated as inner rebar cage and outer rebar cage for the box, at the location of rebar in the actual box. These parts were meshed by surface elements after embedding them in concrete.

### Embedded Element

This is a technique used to place embedded node(s) at desired locations with the constraints on translational degrees-of-freedom on the embedded element by the host element. Both the rebar cages were modeled as the embedded region in concrete using constraints in the interaction module, and making the concrete the host. Thus, rebar elements can only have translations/rotations equal to those of the host elements surrounding them.

### Contact Modeling

Since the boxes were directly placed on the strong reaction floor during the experimental study conducted by Garg et al. (2006) and Abolmaali and Garg (2006), the FEM model and the associated contact analysis procedure were developed to simulate the above condition. Thus, the nonlinear contact analysis procedure was used in modeling the contact between the box and the strong reaction floor. These two surfaces form a contact pair. The strong reaction floor was assigned to be the master surface and the outside face of the bottom slab was assigned to be the slave surface. The node-to-surface contact with small sliding analysis procedure was used during analysis. The details of the FEM model are presented in Fig. 1.

### Material

Material properties of concrete and steel were defined by using their standard properties. Density, modulus of elasticity, Poisson’s

ratio, elastic strain, and plastic strain of concrete and steel were incorporated. For concrete a density of 2,400 kg/m<sup>3</sup> (150 pcf), modulus of elasticity of 27,579 MPa (4,000 ksi), Poisson's ratio 0.17, and total strain 0.003 were used. For steel a density 7,850 kg/m<sup>3</sup> (490.0 pcf), modulus of elasticity 200,000 MPa (29,000 ksi), and Poisson's ratio of 0.3 were used. Steel was presumed as bilinear for modeling purposes with a yield stress of 413.7 MPa (60 ksi).

### Smearred Crack Model

This model was chosen to represent the discontinuous microcrack behavior of concrete. The model does not track individual macrocracks, rather constitutive calculations are performed independently at each integration point of the finite-element model, and the presence of cracks enters into these calculations in the manner that the cracks affect the stress and the material stiffness associated with the model. This modeling approach inherently introduces mesh sensitivity in the solutions, resulting in non-convergence to a unique result. The presence of rebar helps the model to converge as the element does not lose entire stiffness on cracking.

The responses of concrete in compression and cracking, incorporated in the model, are illustrated by the uniaxial response (ABAQUS 2006).

### Tension Stiffening

It is assumed that the material loses strength through a softening mechanism and that this is dominantly a damaging effect. Alternatively opening of cracks can be represented by the loss of elastic stiffness. The model neglects any permanent strain associated with cracking; that is, we assume that the cracks can close completely when the stress across them becomes compressive.

Tension stiffening (ABAQUS 2006, Version 6.6) is required in the concrete smeared cracking model. It is specified by means of a postfailure stress-strain relation.

Tension stiffening is defined as plastic strain at which the cracking stresses causing tensile failure of the concrete reduce to zero. This reduction of tensile cracking stresses with plastic strain can be linear or multilinear. There is a direct relationship between the stiffness degradation and stress drop after cracking (ABAQUS 2006).

In ABAQUS (2006), the failure stress,  $\sigma_f^u$ , occurs at a failure strain (defined by the failure stress divided by the Young's modulus); however, the stress goes to zero at an ultimate strain ( $\epsilon^{\max}$ ). The gap between failure strain and ultimate strain controls the stiffness of the model. This value was calibrated based on the experimental observation which was varied from 0.001 to 0.005. For the brick model, the tension stiffening (TS) was between 0.05 and 0.07. The model was inherently stiff after using reduced integration and the finest possible mesh, therefore TS parameters for the brick elements have to be adjusted in order to capture the true experimental behavior.

### Shear Retention

With crack formation concrete loses shear stiffness. This effect is defined by specifying the reduction in the shear modulus as a function of the opening strain across the crack. One can also

specify a reduced shear modulus for closed cracks. This reduced shear modulus will also have an effect when the normal stress across a crack becomes compressive. The new shear stiffness will have been degraded by the presence of the crack.

The modulus for shearing of cracks is defined as  $\rho G$ , where  $G$ =elastic shear modulus of the uncracked concrete and  $\rho$  =multiplying factor. The shear retention model assumes that the shear stiffness of open cracks reduces linearly to zero as the crack opening increases

$$\rho = (1 - \epsilon/\epsilon^{\max}) \quad \text{for } \epsilon < \epsilon^{\max}, \quad \rho = 0 \quad \text{for } \epsilon \geq \epsilon^{\max} \quad (1)$$

where  $\epsilon$ =direct strain across the crack and  $\epsilon^{\max}$ =user-specified value.

### Failure Ratios

To define the concrete smeared crack model the following ratios were defined in ABAQUS:

1. Ratio of the ultimate biaxial compressive stress to the uniaxial compressive ultimate stress. A value of 1.16 was used;
2. Absolute value of the ratio of uniaxial tensile stress at failure to the uniaxial compressive stress at failure. A value of 0.085 was used initially, but calibrated later;
3. Ratio of the magnitude of a principal component of plastic strain at ultimate stress in biaxial compression to the plastic strain at ultimate stress in uniaxial compression. A value of 1.28 was used; and
4. Ratio of the tensile principal stress value at cracking in-plane stress, when the other nonzero principal stress component is at the ultimate compressive stress value, to the tensile cracking stress under uniaxial tension. A value of 0.333 was used.

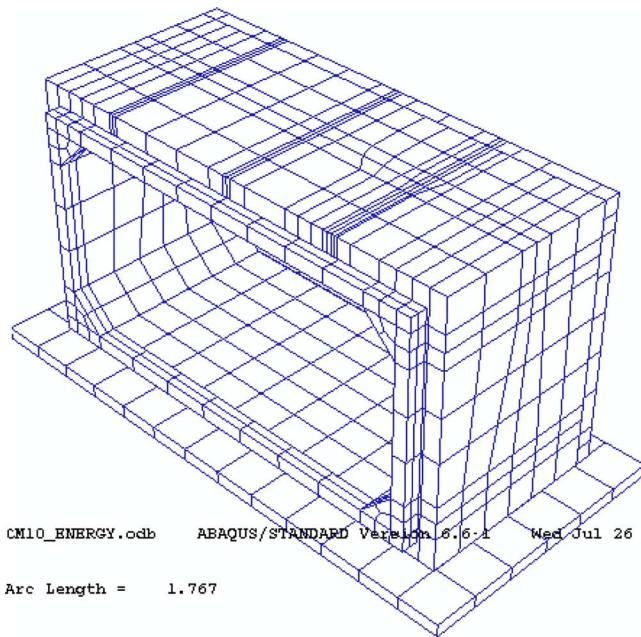
### Modified Riks Analysis Procedure

During cracking of concrete, a local region softens while the adjoining material unloads elastically. These local effects may be accompanied by a sudden change in load keeping displacement constant or a sudden change in displacement keeping the load constant. To obtain nonlinear static equilibrium solutions for unstable problems, where the load-displacement response can exhibit this type of behavior, the modified Riks method (ABAQUS 2006, Version 6.6) was used which is an analysis procedure that allows effective solution of such cases.

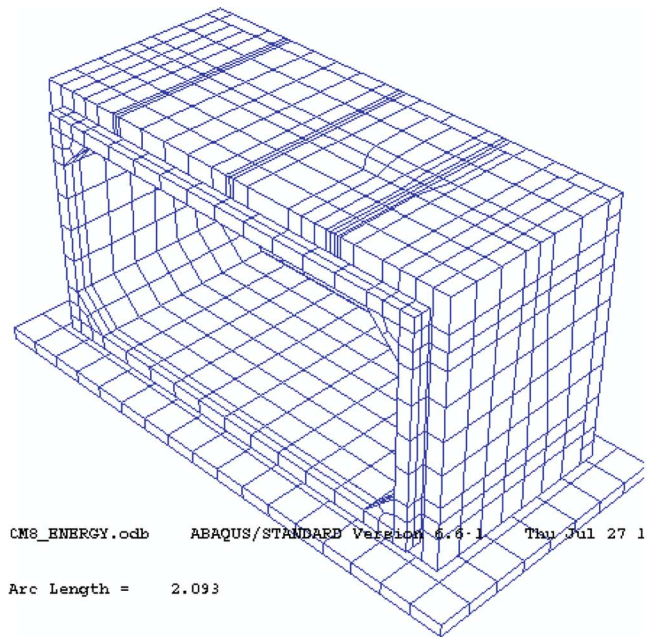
By using the Newton method, an automatic load increment was applied. If the solution did not converge then the increment was reduced by a certain predetermined ratio. Again, the solution was checked and if convergence was not achieved, the process was repeated for a number of predefined iterations or until the solution converged, whichever was earlier (ABAQUS 2006).

### Model Convergence

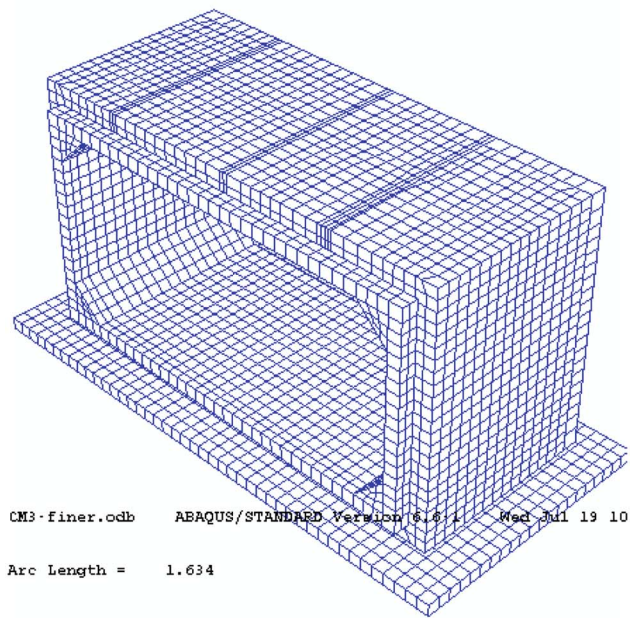
The box designations were defined as: SP or BL\_S-R-L\_N or Y\_lx where the designations are as follows: SP=spigot end; BL=bell end; S-R-L=dimension of the culvert in cm (ft) (span, rise, and the joint length); N=no distribution reinforcement ( $A_{sg}$ ); lx=distance between the tip of the haunch to the edge of the load plate; and Y=with distribution reinforcement ( $A_{sg}$ ) terms of d.



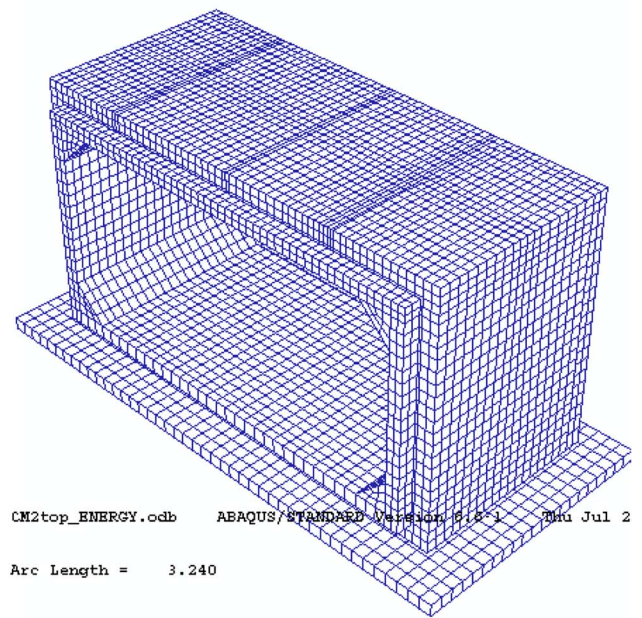
(a)



(b)



(c)



(d)

**Fig. 2.** Various mesh densities: (a) Mesh 1: 1,055 elements and 1,990 nodes; (b) Mesh 2: 1,427 elements and 2,596 nodes; (c) Mesh 7: 10,216 elements and 14,426 nodes; and (d) Mesh 8: 16,166 elements and 21,713 nodes

For example SP\_244-122-122\_Y\_d (SP\_8-4-4\_Y\_d), identifies a spigot-end culvert test with the dimensions of: span = 244 cm (8 ft); rise = 122 cm (4 ft), and joint length = 122 cm (4 ft) with distribution steel  $A_{S6}$ . The edge of the load plate for this test was located at the distance  $d$  from the tip of the haunch.

Various mesh sizes are shown in Fig. 2 for a SP\_244-244-122\_N\_d (SP\_8-4-4\_N\_d) model. These figures show the number of elements and nodes in a given model. Element size decreases with the coarse mesh [Fig. 2(a)] to the finest mesh [Fig. 2(d)]. The numbers of elements in the coarsest and finest models were

1,055 and 16,166, respectively. Energy convergence was sought due to the nonlinear nature of the problem and the fact that monotonic convergence of nonlinear problems based on mesh density refinement alone is not guaranteed (Razavi 2004). The error in energy (external work done—strain energy density) was plotted against the number of elements in the typical boxes SP\_244-122-122\_N\_d (SP\_8-4-4\_N\_d) (Fig. 3). In this figure, the energy error for service load, design load, and loads up to 75 kip decreases as the mesh density increases, and it then becomes stable as mesh becomes finer. While the energy error increases with the increased

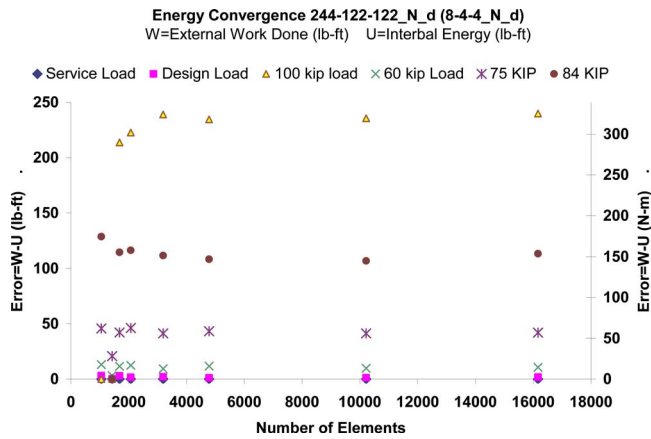


Fig. 3. Typical energy convergence

mesh density for 100 kip load due to the formation of macro-cracks, it also becomes stable with the increased mesh density. The coarsest model, in which the error in energy is insignificant in the subsequent mesh with increased element number, was selected for further analysis. Thus, the mesh with 1,427 elements of Fig. 2(b) was selected.

### Typical Finite-Element Results

The output database files in ABAQUS were read by a visualization module to create contour plots, animations, XY plots, and tabular output of the results. Cracks are not supported by a visualization mode requiring a data file to be read in, which identifies the cracked elements and the level of stress at that point. Alternatively, strain contour is plotted in the visualization mode with the limits of cracking: compressive and tensile strains.

### Deflected Shape

Upon the application of load through the load plate on the outside face of the top slab at the distance  $d$  from the tip of the haunch, the box undergoes deflection. The top and bottom slabs deflect toward the inside of the box and the side walls deflect toward the outside of the box. Fig. 4 shows the deformed shape (solid) compared to the undeformed shape (wire frame) of the SP\_244-122-122\_N\_d (SP\_8-4-4\_N\_d) box, at a load of 356 kN (80 kip). The deformation is magnified 50 times.

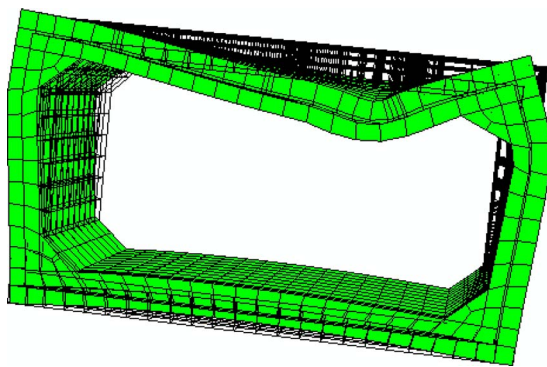


Fig. 4. Typical deflection shape of box: (solid) deformed; (wire-frame) undeformed

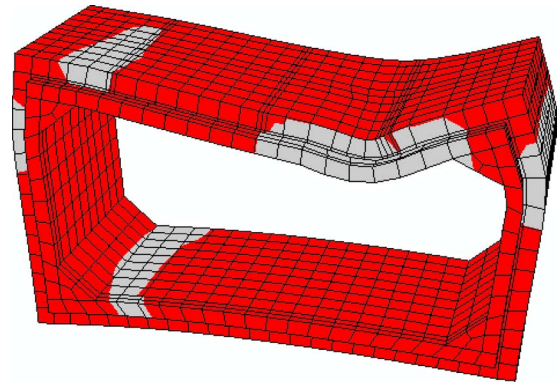


Fig. 5. Typical contours for cracking strain (cracked region: grey color)

### Crack Strain Contours

The contours of the cracking strain on the SP\_244-122-122\_N\_d (SP\_8-4-4\_N\_d) box surface are shown in the Fig. 5 at a load of 356 kN (80 kip). Once again, the deformation is magnified to 50 times. The limit to strains in compression as well as in tension is provided, so that the parts of the box having strains beyond these limits are identified as cracked in compression and tension. This figure shows that cracking at locations of the maximum sagging and hogging moments on the top slab, bottom slab, and both walls will cause tensile cracks. The cracked and intact portions are shown in grey and black, respectively.

### Bending Moment Contours

The contours of the values of moment for a typical box surface are shown in Fig. 6 at a load of 178 kN (40 kip) with a magnification factor of 50. The maximum moments shown are 572 N m (5,060 lb in.) and  $-1,105$  N m ( $-9,779$  lb in.). This figure shows that the maximum sagging moment under the load plate and maximum hogging moment near the left haunch are located on the loading end. With these contours, the values and location of the moments at every load step were known and studied to understand the behavior of the culvert at every load step.

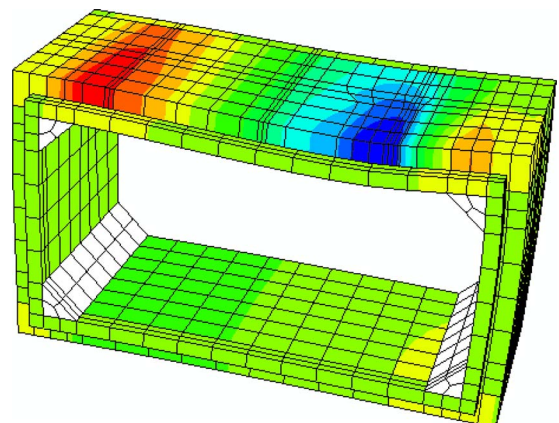


Fig. 6. Typical contours for moment

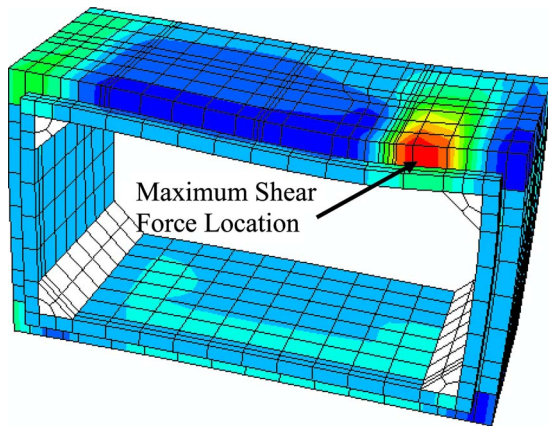


Fig. 7. Typical contours for shear force

### Shear Force Contours

The contours of shear force for a typical box surface are shown in Fig. 7 at a load of 178 kN (40 kip) with magnification factor of 50. The maximum absolute value of shear force is 7,575 N (1,703 lb). It shows that maximum shear force is detected between the load plate and the tip of the haunch at the loading end.

Using the FEM model developed, an investigation was conducted to identify the location of the maximum shear force in the culverts when the wheel load is placed at the distance  $d$  from the tip of the haunch. Table 1 presents the location of the maximum shear force obtained from the FEM analyses of the ASTM C1433 boxes measured from the tip of the haunch for different span sizes. From the values presented in the table, it is noted that the maximum shear force falls between the tip of the haunch and the load plate. It is interesting to note that in 70% of the cases the maximum shear force falls at 1/2 the distance between the tip of the haunch and the edge of the load plate. In only one of the cases [122 cm (4 ft) span] is the maximum shear force under the load plate.

### Model Parameters

Stress locking behavior is inherent in the displacement-based FEM, which introduces a stiffer model compared to the actual

Table 1. Location of Peak Shear along Span, When Load at Distance ( $d$ ) from Tip of Haunch

$S$ [cm (ft)]	$e/d^a$
91 (3)	1.05
122 (4)	1.20
152 (5)	0.50
182 (6)	0.50
213 (7)	0.50
244 (8)	0.50
274 (9)	0.38
305 (10)	0.50
335 (11)	0.50
366 (12)	0.50

Note: Load location ( $d$ ) from tip of haunch.

<sup>a</sup> $D$ =effective depth of top slab;  $e$  distance of peak shear from tip of haunch.

Table 2. Model Calibration Parameters

Test	Modulus of elasticity kN/mm <sup>2</sup> (ksi)	Absolute value of the ratio of uniaxial tensile stress at failure to the uniaxial compressive stress at failure ( $f_t/f'_c$ )	Tension stiffening (TS)
SP_122-122-244_Y_d (SP_4-4-8_Y_d)	20.7 (3,000)	0.0340	0.0015
BL_122-122-244_Y_d (BL_4-4-8_Y_d)		0.0425	0.0010
SP_244-122-122_Y/N_d (SP_8-4-4_Y/N_d)		0.0850	0.0015
BL_244-122-122_Y/N_d (BL_8-4-4_Y/N_d)		0.0640	0.0015
SP_244-122-244_Y_d (SP_8-4-8_Y_d)		0.0510	0.0020
BL_244-122-244_Y/N_d (BL_8-4-8_Y/N_d)		0.0340	0.0020
SP_366-122-122_Y/N_d (SP_12-4-4_Y/N_d)		0.0340	0.0025
BL_366-122-122_Y/N_d (BL_12-4-4_Y/N_d)		0.0170	0.0050
SP_91-61-145_Y_0 (SP_3-2-4.75_Y_0)		0.0425	0.0015
SP_91-61-145_Y_0.85d (SP_3-2-4.75_0.85_Y_0.85d)		0.0340	0.0015

behavior (Rots and Blaauwendraad 1989). Thus, the experimentally obtained load-deflection plots (Garg et al. 2006; Abolmaali and Garg 2006) are compared with the FEM analysis. The parameters calibrated to neutralize the stress locking behavior were: modulus of elasticity of concrete,  $E$ , the absolute value of the ratio of uniaxial tensile stress at failure to the uniaxial compressive stress at failure,  $f_t/f'_c$ , and the tension stiffening parameter TS.

Table 2 shows the values of the aforementioned parameters used for the calibration of the models. The calibrated parameters are compared with the standard parameters of modulus of elasticity ( $E$ )=27.6 kN/mm<sup>2</sup> (4,000 ksi), and absolute value of the ratio of uniaxial tensile stress at failure to the uniaxial compressive stress at failure=0.085.

### Comparison of Experimental and FEM Results

A comparison of the FEM and the experimental results for crack initiation and propagation of cracks showed close correlation. The crack predictions by the FEM analyses using a model comprised of brick elements were similar to those observed in the experiments for the particular load level and crack location shown by Garg (2007).

The FEM analysis generally predicts cracks initially on the inside face of the top slab at the loading end and with the increase in load; the cracks are detected on the outside face of the side walls as shown in Fig. 8. With further increase in load, cracks are predicted on the outside face of the top slab. Similar behavior was observed in the 24 full-scale tests (Garg 2007).

For the test designated SP\_244-122-122\_N\_d (SP\_8-8-4\_N\_d)

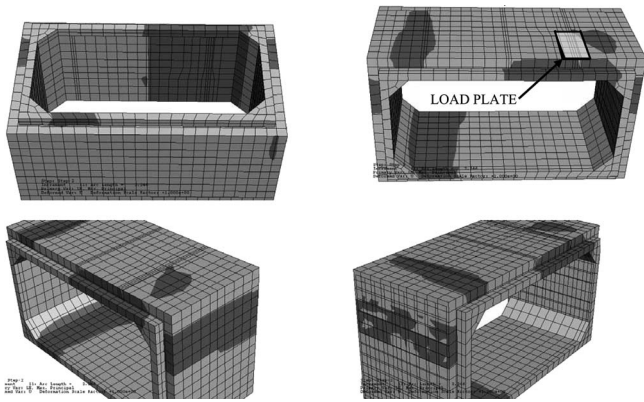


**Fig. 8.** FEM Crack prediction of Model SP\_244-122-122\_N\_d (SP\_8-4-4\_N\_d)

tested on the spigot end, FEM predicts a crack on the inside face of top slab at a load of 169 kN (38 kip), which is confirmed in the test as 187 kN (42 kip) and also presented in experimental photographs of Fig. 9.

Next, the FEM predicted the crack at the outside face of the top slab on the top of the haunch and the outside face of the right wall near the load plate (Fig. 8) at 222 kN (50 kip), which was found experimentally at 222 kN (50 kip) for the side wall and 231 kN (52 kip) for the top slab which are shown in Fig. 9.

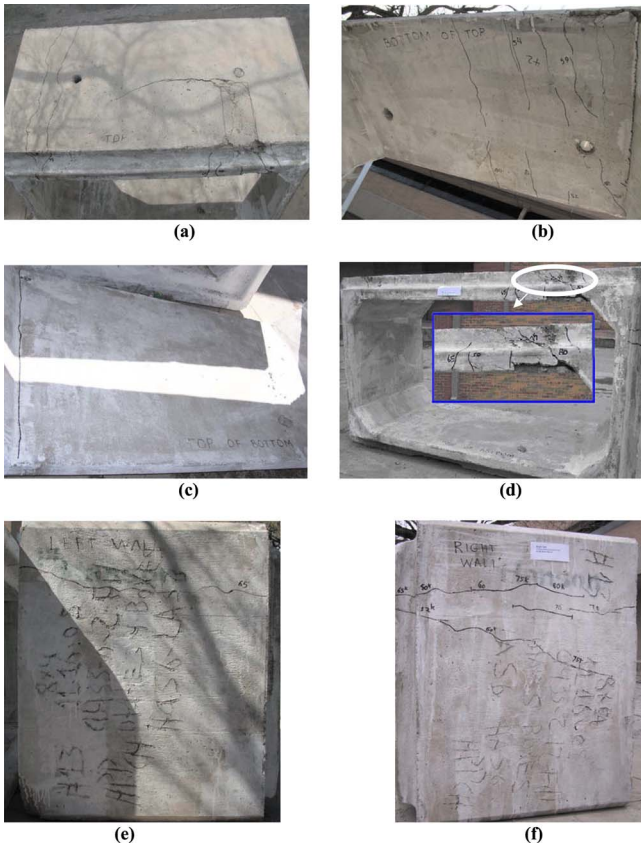


**Fig. 9.** Experimental photograph for test: SP\_244-122-122\_N\_d (SP\_8-4-4\_N\_d): (a) outside face of top slab; (b) inside face of top slab; (c) inside face of bottom slab; (d) spigot end; (e) outside face of left wall; and (f) outside face of right wall

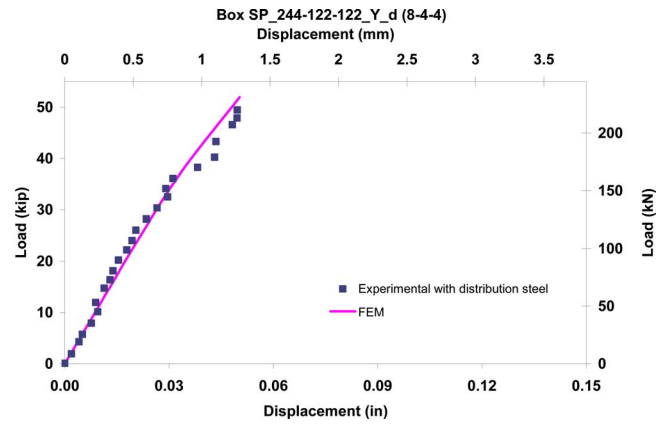


**Fig. 10.** Comparison of FEM with experimental data for SP\_244-122-122\_Y\_d (SP\_8-4-4\_Y\_d)

The FEM crack prediction was continued to the outside face of the left wall (Fig. 8) at 276 kN (62 kip) which was similar to the experimentally observed crack at 289 kN (65 kip) as shown in Fig. 9. Also FEM predicted the crack at the joint between the bottom slab and the left haunch at 383 kN (86 kip). The same phenomenon was observed during the experiment at 289 kN (65 kip).

Comparisons of the typical FEM load-deflection plots versus experimental data are shown Figs. 10 and 11 for SP\_244-122-122\_Y\_d (SP\_8-4-4\_Y\_d) and SP\_244-122-244\_Y\_d (SP\_8-4-8\_Y\_d), respectively. These figures also show a close relationship between the FEM and experimental results.

## Conclusion

A complete detailed three-dimensional FEM of the box culvert per ASTM C1433 was developed and analyzed. Three-dimensional shell and solid elements were used to model the culvert systems. The welded wire fabrics were modeled as rebar elements placed on the surface elements provided by ABAQUS software. The contact surface between the outside face of the bottom slab and reaction floor was modeled by using the nonlinear node-to-surface contact analysis procedure. The analysis procedure consisted of an incremental loading history to capture the nonlinear effects. A smeared crack model along with the Riks

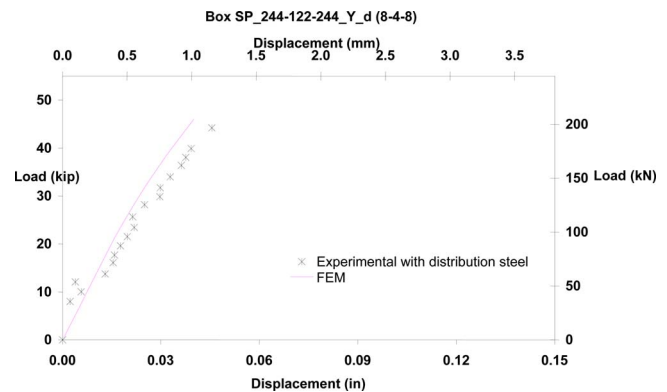


**Fig. 11.** Comparison of FEM with experimental data for SP\_244-122-244\_Y\_d (SP\_8-4-8\_Y\_d)

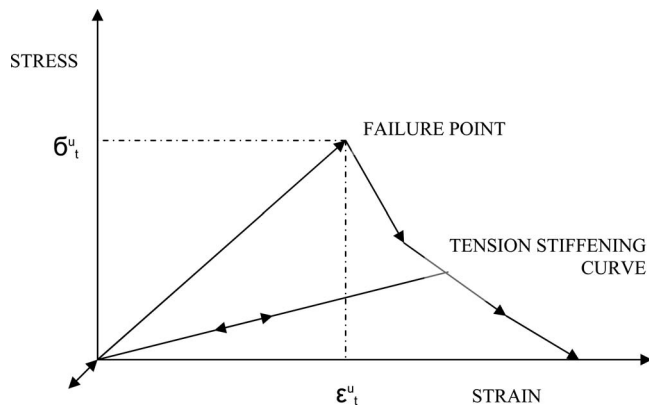


Fig. 12. "Tension stiffening" model

analysis procedure were incorporated to analyze the system for microcracks and to stabilize the solution, respectively. The converged solution was obtained by using  $H$  convergence coupled and an energy-based convergence (see Fig. 12).

The FEM analysis predicted the cracks initially on the inside face of the top slab at the loading end and with the increase in load. The cracks were also detected on the outside face of the side walls. With further increase in load, cracks were predicted on the outside face of the top slab. Shear cracks were observed at the tip of the haunch, at almost twice the factored load as per AASHTO. Similar behavior was observed in the experimental investigation conducted by Garg et al. (2006) and Abolmaali and Garg (2006).

The load-deflection plots obtained from the FEM analyses were compared with those obtained from the experimental results, which showed close correlations. The model thus obtained is used to study the behavior of reinforced box culverts per ASTM C 1433 by Abolmaali and Garg (2008b) and Garg (2007).

## Acknowledgments

The financial support of the National Science Foundation, Federal Highway Institute, and the American Concrete Pipe Association are gratefully acknowledged

## References

- ABAQUS. (2006). *ABAQUS manual*, Version 6.6, Pawtucket, R.I.
- Abolmaali, A., and Garg, A. K. (2006). "Failure mode for precast concrete box culverts subjected to wheel live load." *Proc., Transportation Research Board 86th Annual Meeting (CD-ROM)*, Transportation Research Board, Washington, D.C.
- Abolmaali, A., and Garg, A. K. (2008a). "Effect of wheel live load on shear behavior of precast reinforced concrete box culverts." *J. Bridge Eng.*, 13(1), 93–99.
- Abolmaali, A., and Garg, A. K. (2008b). "Shear behavior and mode of failure for ASTM C 1433 precast box culverts." *J. Bridge Eng.*, 13(4), 331–338.
- ASTM. (2003). "Standard specification for precast reinforced concrete box sections for culverts, storm drains, and sewers." *C1433-03*, West Conshohocken, Pa.
- Garg, A. K. (2007). "Experimental and finite element-based investigations of shear behavior in reinforced concrete box culverts." Doctor of Philosophy, Ph.D. dissertation, Univ. of Texas at Arlington, Arlington, Tex.
- Garg, A. K., and Abolmaali, A. (2006). "Shear behavior of small span single and double precast reinforced concrete box culverts." *Proc., Pipelines 2006, Service to the Owner (CD-ROM)*, ASCE, Reston, Va.
- Garg, A. K., Abolmaali, A., and Fernandez, R. (2006). "Experimental investigation of shear capacity of precast reinforced concrete box culverts." *J. Bridge Eng.* 12(4), 511–517.
- Razavi, H. (2004). "Kinematic hardening cyclic plasticity-based semi-meshless finite element analysis procedure for contact and bolted problems in computational mechanics." Doctor of Philosophy, Ph.D. dissertation, Univ. of Texas at Arlington, Arlington, Tex.
- Rots, J. G., and Blaauwendraad, J. (1989). "Crack models for concrete: Discrete or smeared? Fixed, multi-directional or rotating?" *Heron*, 34(1), 45–49.